J Mater Sci (2007) 42:9565–9571
DOI 10.1007/s10853-007-1816-2

INTERFACE SCIENCE

Surfactant-assisted synthesis and characterization of lanthanum oxide nanostructures

Jie Sheng · Shuang Zhang · Sa Lv · Wendong Sun

Received: 9 March 2007 / Accepted: 1 May 2007 / Published online: 10 July 2007

Abstract By a simple hydrothermal process, we have synthesized lanthanum oxide nanoneedles, nanorods, and nanorod bundles. The porosity of the obtained materials was found. The structure and morphology of the maintained products were studied by XRD, TG/DTA, TEM, and SAED. The porosity was illustrated by N_2 absorption–desorption, BET, and BJH curves. Moreover, the influence factors and the mechanism for the morphology control of lanthanum oxide have also been preliminarily presented.

Introduction

Since Iijima discovered Carbon nanotubes with High-resolution transmission electron microscope (HRTEM) in 1991 [1], one-dimensional nanomaterial have attracted intensive attention because of their potential applications in nanoconnectors and nanodevices [2]. To possess enhanced electrical, magnetic, optical, and mechanical properties, these 1D materials need to be of small diameter, high aspect ratio, and uniform orientation [3]. The synthesis and functionalization of 1D nano-structural materials has become one of the most highly energized research areas [4–6]. Until now, many attempts have been made to fabricate 1D nanostructure materials such as carbon nanotubes, metals, semiconductors, and conductive polymer nanorods or nanowires [7–10]. Many methods, such as e-beam lithography [11], sol–gel method [12], laser ablation [13], chemical vapor deposition [14] and template method [15, 16] have been used for the preparation of nanorods or nanowires. However, to our knowledge, complex process control, high reaction temperatures or long synthesis time may be required for these approaches. The introduction of hydrothermal process has provided a relatively simple and powerful method of the synthesis of nanoparticles and nanorods/wires. Compared with those methods, hydrothermal process has the following advantages: (a) effective control of size and shape of the particle; (b) shorter preparation time; (c) fewer impurities in the final product. So hydrothermal method is widely used to prepare the nanostructure materials [17–21].

Lanthanide oxide materials have also received increasing attentions because they can be extensively as piezo-electricity materials, galvanothermy materials, thermoelectricity materials, an important component in automobile exhaust-gas convectors, catalyst support [22–24]. In addition, lanthanide oxides are currently the subject of intense research efforts directed towards the creation of solid fuel cells [25], novel high temperature superconductors [26], and nano-scale self-assemblies [27]. In the future, the exploitation of such lanthanide oxide architectures may provide the opportunity for producing innovative ceramic materials with novel and tunable magnetic, electronic, or catalytic properties [28, 29]. The synthesis of porous material may provide an effective means of generating architectures of this kind. If lanthanide oxides were prepared in 1D nanostructure, they would hold promise as highly functionalized materials as a result of both shape-specific and quantum size effects [30]. As a consequence, numerous techniques have been proposed to synthesis lanthanum particles with promising control of properties, such as thermal decomposition [31], super-molecular template route [32], micelles [33], homogenous precipitation

J. Sheng · S. Zhang · S. Lv · W. Sun (✉)
Department of Chemistry, Northeast Normal University, 5268 Renmin Street, Changchun, Jilin 130024, PR China
e-mail: sunwd843@nenu.edu.cn

route [34], etc. Recently, Vadivel Murugan et al. reported microwave hydrothermal synthesis of Eu^{3+} doped lanthanum oxide nanowhiskers [35] and concluded that MH preparation plays an important role affecting the morphology.

In our work, we present a surfactant-assisted hydrothermal method to synthesis lanthanum oxide materials for the first time using cationic surfactant CTAB as template agent and lanthanum chloride as precursors. The obtained nanorod is of small diameter, and high aspect ratio (5–15 nm in width and 200–400 nm in length). Meanwhile the porous structure in lanthanum oxide was found, and this structure still maintained after surfactant removal by simple air calcinations at 450 °C. In this paper, the influence factors and the mechanism for the morphology control of lanthanum oxide have also been discussed.

Experiment

The materials used in the work included Lanthanum chloride ($LaCl_3{\cdot}6H_2O$), hexadecyltrimethyl-ammonium bromide (A.R, Sinopharm Chemical Reagent Co Ltd., Shanghai, China), ammonia (25%, Beijing Chemical Reagent Co Ltd., Beijing, China). Apparatus used in the work included X-ray diffractometer (2200VPC, Rigaku Ltd., Japan), Transmission electron microscopy (H-800, Hitachi Ltd, Japan; JEM-2010, JEOL, Japan), Micrometrics NOVA-1000 apparatus (Quantachrome Corp, American), SDT 2960 thermo-gravimetric apparatus (TA Instrument, USA).

Sample preparation

All of the reactants were analytical grade and used without any further purification. The synthesis of La_2O_3 nanorods was carried out as follows: 0.2730 g of hexaclecylerimethylammonium bromide (CTAB) was first put into 30 mL distilled water under magnetic stirring at room temperature. Then 0.5860 g Lanthanum chloride ($LaCl_3{\cdot}6H_2O$) was added with stirring to form a homogeneous transparent solution, and 0.1–0.6 mL 25% ammonia was added dropwise to the above solution to adjust the pH value of the solution from 6.0–10.0. Along with the addition of ammonia, the solution was turned translucent colloidal right now. After vigorous stirring for 2 h, the system was transferred into a Teflon lined stainless steel auto clave, sealed and maintained at 80 °C for 24 h. Subsequently, the resultant white solid product was centrifuged, washed with distilled water and ethanol to remove the ions possibly remaining in the final product and finally dried at 60 °C in air.

Characterization

The as-prepared powder samples were characterized by X-ray powder diffraction (XRD) on a Rigaku X-ray diffractometer with Cu$K\alpha$ radiation (λ = 1.5406 Å). The morphology and size of as-obtained product were observed by transmission electron microscopy (TEM, Hitachi H-800). Selected area electron diffraction (SAED) was performed with transmission electron microscope (JEOL JEM-2010, 200 kV). The porous structure properties of the sample were determined with a micrometrics NOVA-1000 apparatus by using nitrogen as the analysis gas. The TG/DTA curves were determined on a SDT 2960 thermogravimetric apparatus in nitrogen with a heating rate of 10 °C/min.

Result and discussion

TG/DTA analysis

The result of thermal analysis for lanthanum oxide nanorods is presented in Fig. 1. In the TG/DTA curve, below 200 °C, the weight loss is about 2.1%. It is attributed to the loss of the absorbed water. The DTA peak of 380 °C is corresponding to a loss of the residual water and the surfactants and the weigh loss is 9.2%. The peak between 400 °C and 500 °C is possible resulted by unhydrolyzed lanthanum chloride reaction [36].

$$LaCl_3 \cdot 6H_2O = LaOCl + 2HCl + 5H_2O.$$

The peak between 500 and 700 °C may result from the removal of the residual surfactants and the decomposition of $La(OH)_3$ [35].

$$2La(OH)_3 \rightarrow 2LaO(OH) + 2H_2O \rightarrow La_2O_3 + H_2O.$$

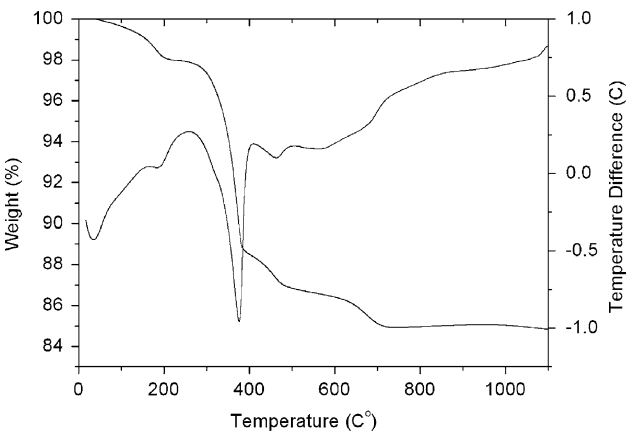

Fig. 1 TG/DTA curves obtained for rod-like phase lanthanum oxide

Up to 850 °C, the total weight loss is about 15%. These results show that the surfactants can be removed by calcinations at 850 °C.

X-ray diffraction measurement

X-ray diffraction measurement was carried out to investigate the composition and phase structure of obtained samples. Because samples with different shapes all give similar XRD patterns, we only show that of rod-like products as example. Figure 2 is the XRD patterns of the sample calcined for 2 h at 450 and 850 °C, respectively. Figure 2a shows the diffraction peaks of La_2O_3 and LaOCl, which indicate the possibility of unhydrolyzed lanthanum chloride reaction. The space value of the sharp peak at 29.90° is 2.986, which is in accordance with the literature value 2.981 at 29.95 of La_2O_3. In Fig. 2b, most of the peaks can be readily indexed as hexagonal La_2O_3 structure (JCPDS card no. 73–2141). The strong and broaden peaks indicate that the material has good crystallization and small size.

TEM

The morphology of product was determined by TEM. Figure 3a shows typical TEM images of as-prepared product obtained using 0.3 mL $NH_3{\cdot}H_2O$ (pH ≈ 8.5). From the figures we can see that the product is mainly composed of La_2O_3 nanorods, and the nanorods are 5–15 nm in diameter and 200–400 nm in length. The SAED pattern (the inset in Fig. 3a) recorded with the electron beam perpendicular to the long axis of the hexagonal structured La_2O_3 nanorod and the highly symmetrical dotted lattice in ED pattern reveals the single crystal nature of rod-like La_2O_3. When the amount of $NH_3{\cdot}H_2O$ was decreased from 0.3 to 0.1 mL (pH ≈ 6.0), while keeping the other conditions constant as that for La_2O_3 nanorods, the products were La_2O_3 nanoneedles, as shown in Fig. 3b. With increasing the amount of $NH_3{\cdot}H_2O$ from 0.3 to 0.6 mL (pH ≈ 9.0), the morphology of product was nanorods parallel and nanorods bundles, as demonstrated in Fig. 3c,d. ED pattern inset in Fig. 3d corresponding to the La_2O_3 nanorod bundles.

Based on the above results, it could be concluded the lanthanum oxides nanostructure with different morphologies could be obtained in micelle solution with different pH values. Researchers have also synthesized hexagonal, cubic and lamellar mesostructured silica MCMs, V–P, and Al–B oxides in the different micelle solution phases by adjusting pH value of the solution [37–39]. A conclusion can be drawn from these works that the micelle structures of surfactant will change with increasing pH value, which results in the formation of the products with different structures. In our experiment, from a mass of data we found that only 1D La_2O_3 nanostructures but not other morphologies mentioned above were obtained. We think that this is possibly resulted from the morphology of the CTAB micelle. Under our experimental conditions, 1D acerate and claviform micelle structures will be formed in the solution when CTAB was dissolved in water, which results in the formation of 1D morphology of final product. Besides, it has also been considered that the higher pH value is used, the higher degree of the condensation between precursors occurs [33]. With the increase in framework densification, a consequent phase change in the surfactant micelle packing would occur, leading more stable claviform rather than acerate phases. So the pH value of the reaction system has a little effect for the formation of these products.

Figure 4 presents the morphology of La_2O_3 nanorods prepared at different reaction temperature. As can be seen, when the reaction temperature was maintained at 40 and 60 °C, respectively, and the other conditions were the same as that for La_2O_3 nanorods, La_2O_3 nanorods grew longer with increasing the reaction temperature. At 40°C (Fig. 4a), La_2O_3 were nanorods dispersed uniformly with the length being about 120 nm. When the reaction temperature was kept at 60 °C (Fig. 4b), La_2O_3 nanorods were observed clearly with the length being about 200 nm. Further increasing the reaction temperature to 80 °C (Fig. 3a), the length of the nanorods became longer obviously. The average length could reach 400 nm while the diameter had no apparent change. On the other hand, at a

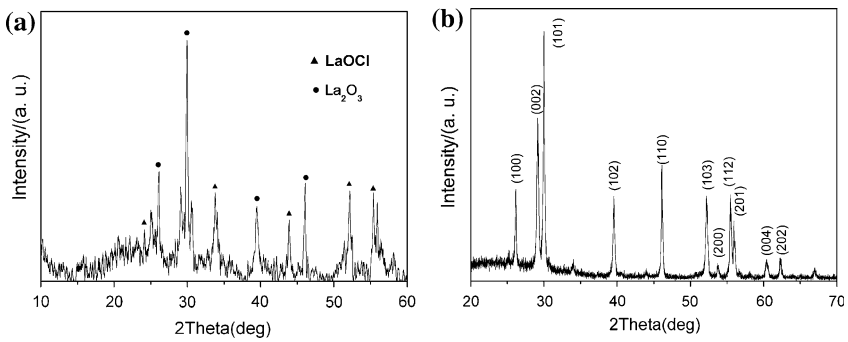

Fig. 2 Typical X-ray diffraction pattern of the as-synthesized products calcined at different temperature. (**a**) 450 °C and (**b**) 850 °C

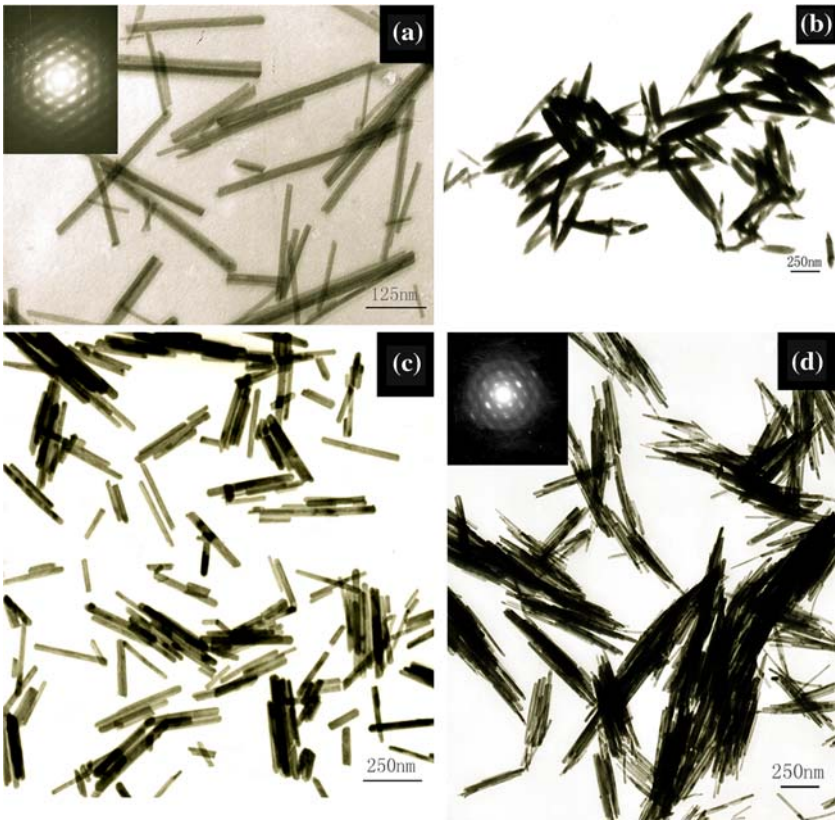

Fig. 3 TEM images of sample obtained at different pH value. (**a**) pH ≈ 8.5. Inset: SAED pattern of a nanorod, (**b**) pH ≈ 6.0, (**c**) pH ≈ 9.0, and (**d**) pH ≈ 10.0. Inset: SAED pattern of nanorod bundles

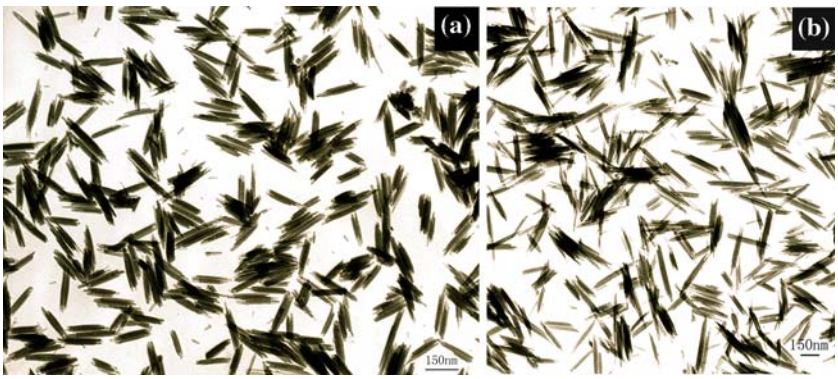

Fig. 4 TEM images of sample obtained at different temperature. (**a**) 40 °C and (**b**) 60 °C

lower temperature, such as 25 °C, there was no precipitate existed. Therefore, it could be concluded that reaction temperature was a key factor influencing the length of nanorods.

Figure 5 shows the images of La_2O_3 nanorods prepared with different reaction time. The figures indicate that the length of the nanorods grows longer with increasing the reaction time. With 8 h (Fig. 5a), we obtained the rods with 85 nm in length and 5 nm in width. When the time rose to 12 h (Fig. 5b), the length of nanorods was 120 nm. When the time reached 24 h, the length turned to 200–400 nm (Fig. 3a). So the reaction time also plays important role influencing the length of nanorods.

The effect of the amount of CTAB on the morphology of the product was shown in Fig. 6a–c. These images show the product obtained with the amount of CTAB at 10 CMC, 100 CMC, and 1000 CMC (CMC represent Critical Micelle Concentration), respectively. From the images we found that with increasing the amount of CTAB, the length of La_2O_3 nanorods reduces, but the diameter of nanorods almost remains unchanged (about 5 nm). They are also very stable in aqueous solution as long as several months with good dispersion. As to the controlling mechanism of CTAB we think there were two folds: First, it is generally believed that micelle is non-sphericity such as ellipsoidal shape, oblate shape, acetabuliform or claviform when the

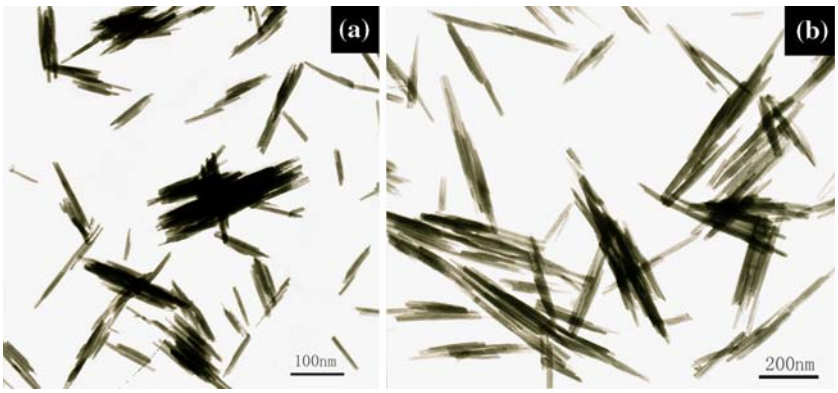

Fig. 5 TEM images of sample obtained at different reaction time. (**a**) 8 h and (**b**) 12 h

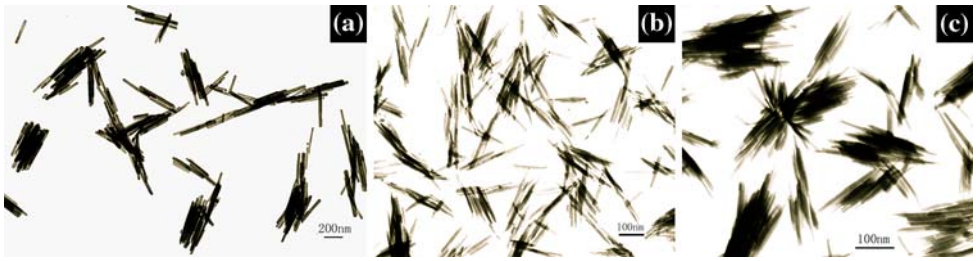

Fig. 6 TEM images of sample obtained at different concentration of the surfactant. (**a**) 10 CMC, (**b**) 100 CMC, and (**c**) 1000 CMC

concentration of surfactant reaches 10 times CMC. The specific shape of micelle depends on the geometric arrange parameter P of the surfactant molecule. P can be calculated using the following formula [40]:

$$P = V_c/l_c A_o$$

where V_c is the volume of hydrophobic group, l_c is the length of hydrophobic group hydrocarbon chain, and A_o is the average occupied area of hydeophilic group arranging tightly in monolayer.

As to CTAB we used in our experiment, the geometric arrange parameter P was in 1/3–1/2, so it could form claviform micelle. When taking the claviform micelle as soft template prepares La_2O_3, the obtained product would be claviform. This is in accordance with the experiment result. In addition, as we known, CTAB is often used as "capping reagent" in nanomaterial fabrication because it can bond to solid surface and selectively adsorb on some specific facets of crystals to control crystal growth direction consequently. With the more surfactant used, the selective adsorption of CTAB probably took place at the nucleation stage, so that the product had very small diameter (about 5 nm).

As for La_2O_3 nanorod, they have the tendency to parallel to each other. The reasons for these rods to align in parallel are two-fold: First, within hard-rod approximation, this side-by-side ordering occurs in order to maximize the entropy of the self-assembled structure by minimizing the excluded volume per particle in the array as first proved by Onsager [41]. Second, the higher lateral capillary forces along the length of a nanorod, as compared with its width, could be another important driving force for the side-by-side alignment of nanorod rather than end-to-end [42]. In short, we discussed the influence factors for the morphology control of lanthanum oxide: the pH values of the micelle solution, reaction time, reaction temperature and the amount of CTAB. Recently, Vadivel Murugan et al. reported microwave hydrothermal reaction to synthesis nano-whisker morphology of Lanthanum oxide [35]. In our work, we also concluded that the synthesis way is an important factor affecting the morphology of the product.

N_2 adsorption–desorption isotherms

The porosity of the sample was found from gas adsorption measurements. Figure 7 shows the typical nitrogen adsorption–desorption isotherms. Surface area and average pore size of lanthanum oxide nanorods calcined at 450 °C are also showed in Table 1. Pore size distribution data is given in Fig. 8.

Both of the resulting isotherms could be identified as type Langmuir III isotherms. In the curve, there is a very clear hysteresis loop, the typical characteristic can be used to illuminate the capillary condensation. BJH analysis shows that the porous La_2O_3 possesses a mean pore diameter of 7.9 nm, and according to BET analysis, the surface area of the product is 84 m^2/g. The sharp peak

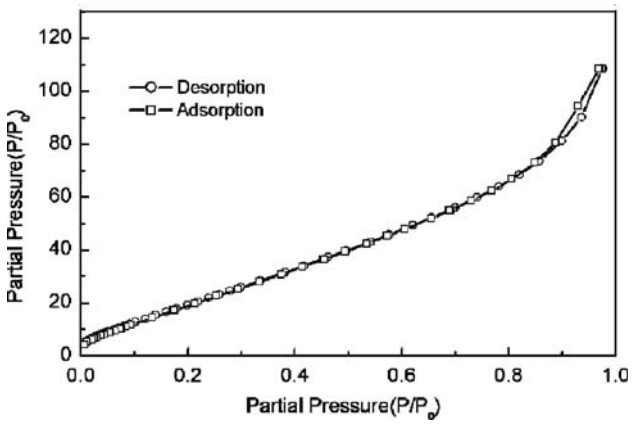

Fig. 7 BET nitrogen adsorption–desorption isotherms for rod-like phase lanthanum oxide

Table 1 Nitrogen sorption data of surface areas and pore diameters, calculated by BET and BJH models, respectively, for lanthanum oxide nanorod following air calcinations at 450 °C

Sample	La_2O_3 nanorods obtained after air calcinations at 450 °C
Surface area, m^2/g	84
Pore diameter, Å	79.368

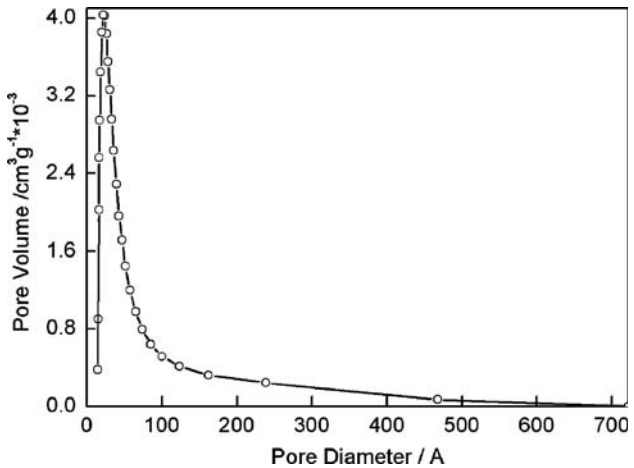

Fig. 8 BJH plot of pore volume versus pore diameter for lanthanum oxide

observed for the sample is consistent with increases in post-calcination disorder of the systems and suggest a less well-defined size distribution.

Conclusion

In summary, by means of the proper control of the reaction conditions and with the assistance of surfactant CTAB, we have successfully prepared La_2O_3 nanoneedles, nanorods, nanorod bundles in aqueous solution. It has been found that the pH values of the micelle solution, reaction time, reaction temperature and the amount of CTAB all play important roles in the formation of La_2O_3 nanocrystals with various morphologies. The porosity materials will provide the opportunities for some potential applications as advanced materials.

References

1. Iijima S (1991) Nature 354:56
2. Fasol G (1998) Science 280:545
3. Holmes JD, Johnston KP, Doty RC, Korgel BA (2000) Science 287:1471
4. Duan X, Huang Y, Garwal RA, Lieber CM (2003) Nature 421:241
5. Fuhrer MS, Nygard J, Shih L, Forero M, Yoon YG, Mazzoni MSC, Choi HJ (2004) Science 288:494
6. Ren Huang ZF, Xu JW, Wang JH, Bush P, Siegal MP, Provencio PN (1998) Science 282:1105
7. Archibald DD, Mann S (1993) Nature 364:430
8. Mmorale AM, Lieber CM (1998) Science 279:208
9. Tang Z, Kotov NA, Giersig M (2002) Science 297:237
10. Ma J, Gu Y, Shi L, Chen L, Yang Z, Qian Y (2003) Chem Phys Lett 381:194
11. Masuda H, Yamada H, Sayoh M (1997) Appl Phys Lett 71:2770
12. Cheng B, Samulski ET (2001) J Mater Chem 11:2901
13. Duan XF, Lieber CM (2000) Adv Mater 12:298
14. Bjork MT, Ohlsson BJ, Sass T, Persson AI (2002) Nano Lett 2:81
15. Fodor PS, Tsoi GM, Wenger LE (2002) J Appl Phys 91:8186
16. Tai YL, Teng H (2004) Chem Mater 16:338
17. Yang Q, Tang K, Wang C, Qian Y, Zhang S (2002) J Phys Chem B 106:9227
18. Zhang J, Yang X, Wang D, Li S, Xie Y, Qian Y (2000) Adv Mater 12:1348
19. Zhang H, Ma X, Li Y, Xu J, Yang D (2003) Chem Phys Lett 377:654
20. Zhang H, Li Y, Ma X, Xu J, Yang D (2003) Nanotechnology 14:974
21. Vayssieres L (2003) Adv Mater 15:464
22. Arakawa H (1994) Bull Chem Soc Jpn 11:21
23. Andriamasinoro D, Kieffer R, Kiennemann A, Poix P (1993) Appl Catal 106:201
24. Rosynek MP, Magnison DT (1977) J Catal 46:402
25. Muttay EP, Tsai T, Barnett SA (1999) Nature (Lond) 400:649
26. Allenspach P, Gasser U (2000) J Alloys Compd 311:1
27. Orr GW, Barbour LJ, Atwood JL (1999) Science 285:1049
28. Tissue BM (1998) Chem Mater 10:2837
29. Terrible D, Trovarelli A, Llorca J, De Leitenburg C, Dolcetti GJ (1998) J Catal 178:299
30. Wu GS, Xie T, Yuan XY, Cheng BC, Zhang LD (2004) Mater Res Bull 39:1023
31. Imanaka N, Masui T, Kato Y (2005) J Solid State Chem 178:395
32. Lyons DM, Harman LP, Morris MA (2004) J Mater Chem 14:1976
33. Cao JM, Ji HM, Liu JS, Zheng MB, Chang X, Ma XJ, Zhang AM, Xu QH (2005) Mater Lett 59:408
34. Yada M, Kitamura H, Ichinose A, Machida M, Kijima T (1999) Angew Chem Int Ed 38:3506
35. Vadivel Murugan A, Viswanath AK, Kakada BA, Ravi V, Saaminathan V (2006) J Phys D Appl Phys 39:3974

36. Chao Y, Quan MJ, Ping LX, Xin W (2003) J Chem Eng Chinese Univ 6:685
37. Huo Q, Margolese DI, Ciesla U, Demuth DG, Feng P, Gier TE, Siege P, Firouzi A, Chmelka BF, Schuth F, Stucky GD (1994) Chem Mater 6:1176
38. Noritaka M, Hiroshi H, Sayaka U, Akira T (2001) Chem Mater 13:179
39. Ayyappan S, Rao CNR (1997) Chem Commun 575
40. Israelachvili JN (1985) Physical principles of surfactant self-association into micells, wesicles and microemulsion droplets. In: Mitall KL, Bothorel P (eds) Surfactant in Solution, New York
41. Vroege GJ, Lekkerkerker HNW (1992) Rep Prog Phys 55:1241
42. Kwan S, Kim F, Akana J, Yang PD (2001) Chem Commun 447